

Dynamic Operation of a Heat Exchanger in a Thermally Integrated Photovoltaic Electrolyzer

Erno Kemppainen,* Rory Bagacki, Christian Schary, Fuxi Bao, Iris Dorbandt, Stefan Janke, Quiterie Emery, Bernd Stannowski, Rutger Schlatmann, and Sonya Calnan

The outdoor operation of an up-scaled thermally photovoltaic electrolyzer (PV EC), constructed using a heat exchanger (HE) made of low-cost materials, compared to its nonintegrated counterpart to quantify heat transfer and its effects, is studied. Thermal coupling of the PV and EC can reduce the difference between their temperatures, benefitting device performance. Such devices can produce hydrogen at rooftop installations of small-to-medium-sized nonindustrial buildings. The devices are tested outdoors using automated real-time monitoring. Under $\approx 880 \text{ W m}^{-2}$ peak irradiance, they produced hydrogen at ≈ 120 and $\approx 110 \text{ mL min}^{-1}$ rate with and without HE, respectively, corresponding to about 8.5% and 7.8% solar-to-hydrogen efficiencies. During about 700 h of testing, the HE is beneficial at over $\approx 500 \text{ W m}^{-2}$ due to cyclic device operation. Under lower irradiance levels, pumping previously heated electrolyte through the HE increases the PV and reduces the electrolyte temperature, reducing the device performance. The HE increases the cumulative hydrogen production ($\approx 800 \text{ L}$ from both devices), so even relatively modest heat transfer rates can improve the PV EC operation. Improving the HE should further increase the benefits, but additional measures may be needed to maximize the hydrogen production.

1. Introduction

While renewable energy sources in principle offer a practically endless supply of energy, their seasonal and diurnal variability necessitates energy storage to enable the large-scale adoption needed to replace fossil fuels as our primary energy source.^[1,2] Solar energy is the largest renewable energy source by a large margin and so its conversion to and storage in a useful form is especially important.^[3] Hydrogen production through water electrolysis is considered a central power-to-fuel technology and has garnered interest as an energy storage method that could significantly contribute to both seasonal energy storage and decarbonization of the transport sector, among other possibilities.^[4,5] While water electrolysis and hydrogen fuel cells are established technologies with commercial applications, the cost of (energy from)

hydrogen is not yet competitive with fossil fuels,^[6,7] hindering the use of hydrogen technologies in commercial and industrial-scale applications and energy storage, and almost all hydrogen is produced from fossil fuels, most by steam methane reforming,^[8] a source of CO_2 emissions. Development of electrolysis and related technologies is thus needed to make renewable hydrogen production an economically viable energy storage method.

Using solar energy to power the electrolysis, for example, with photovoltaics (PV) follows naturally from the wide availability of solar energy and water, and the need for renewable energy storage and a range of device architectures from separate electrolyzer (EC) and PV installations, connected by electricity grid, to fully integrated photoelectrochemical (PEC) and photocatalytic (PC) devices is being developed for this purpose.^[9–11] In recent years, remarkably large examples of PC^[12] and PEC^[13,14] devices have been reported in literature, but, generally, the most mature technologies are the least integrated ones while the most integrated and advanced concepts represent the least mature technologies.


Direct coupling of PV modules to ECs without power electronics is simple, as a concept, but requires careful matching of the PV and EC to each other to maximize the hydrogen yield. From the technological standpoint, it combines relatively mature technologies in a less mature package that is not quite yet ready for

E. Kemppainen, R. Bagacki, C. Schary, F. Bao, I. Dorbandt, S. Janke, Q. Emery, B. Stannowski, R. Schlatmann, S. Calnan
PVcomB
Helmholtz-Zentrum Berlin
12489 Berlin, Germany
E-mail: erno.kemppainen@helmholtz-berlin.de

F. Bao
Currently School of Chemistry and Chemical Engineering
Shihezi University
Shihezi 832003, P. R. China

B. Stannowski
Fac. II - Mathematics, Physics, Chemistry
Berliner Hochschule für Technik (BHT)
13353 Berlin, Germany

R. Schlatmann
Renewable Energy
Hochschule für Technik und Wirtschaft Berlin (HTW)
12459 Berlin, Germany

 The ORCID identification number(s) for the author(s) of this article can be found under <https://doi.org/10.1002/ente.202201081>.

© 2022 The Authors. Energy Technology published by Wiley-VCH GmbH. This is an open access article under the terms of the Creative Commons Attribution License, which permits use, distribution and reproduction in any medium, provided the original work is properly cited.

DOI: 10.1002/ente.202201081

commercial applications, so scaling up and optimization are especially relevant for its development.^[15,16] Due to the low maturity of the integrated technologies, the thermal aspects of the integration are relatively less studied than the separate components. However, research on the topic is ongoing, especially on devices utilizing concentrating optics, as the higher temperature and consequent potential for damage make the thermal aspects of the device more important than without concentrating optics.^[14,17] Generally, thermal integration is considered beneficial for solar-to-hydrogen conversion, and thermally integrated large PV-based devices (area or/and operating power) have been reported and studied with^[14,18] and without^[19,20] light concentration. Additionally, practically all PC and PEC devices are thermally integrated by the virtue of the solid–liquid contact between the photoabsorber and electrolyte. Continuing scale up development from our earlier (thermally uncoupled) 294 cm² prototype,^[21] we now study and report the operation of a thermally integrated PV EC with ≈ 2600 cm² solar collection area. Some preliminary results have already been reported elsewhere,^[22] and this study considers the operation of the PV ECs, especially the heat exchanger (HE) and its effects, in more detail.

Temperature measurements and analysis of some aspects of the thermal operation are quite common, when discussing integrated devices, but more detailed analysis to also quantify the benefits of the integration is rare, and in some cases, a nonintegrated device might not even be feasible. In the case of separate PV and EC, the effect of the HE and some of its details on the hydrogen production has been studied computationally (for a device with a DC–DC converter)^[23] and some aspects of using a separate coolant (i.e., not the electrolyte) to cool the PV and to collect heat also experimentally, but apparently without heating the EC.^[24] These studies indicate that HE should increase the hydrogen production, which is also commonly accepted, but there appear to be no empirical comparisons to quantify heat transfer and its benefits for an integrated PV EC device.

Unlike previous studies discussed above, this contribution directly compares a PV EC device with thermal integration to its unintegrated counterpart. This enables unique insights into

the effects of heat transfer on the PV EC performance and on the transient behavior of the heat transfer itself in outdoor conditions. In addition to reporting the central performance parameters of our PV EC device, we analyze the effect heat transfer on its operation and the benefits of the thermal integration by comparing the simultaneous operation of the thermally integrated PV EC and its nonintegrated counterpart. Therefore, by combining the heat transfer analysis of the integrated device with the comparison to the nonintegrated device, we can quantify the direct effects of the thermal integration on, for example, operating temperatures and the consequences on the hydrogen production rate and the efficiency of the device

2. Description of the Measured PV EC Devices

Both measured PV EC devices were based on a PV module with nine (9) silicon heterojunction (SHJ) cells connected in series, with a total module area of ≈ 2600 cm² (51 cm \times 51 cm bottom plate, **Figure 1a**). The bottom plate of the modules was aluminum to facilitate heat transfer and for mechanical strength. Electrically, both modules were directly connected to a stack of three (3) ECs with 15 cm \times 15 cm electrode area. The liquid alkaline-based ECs were designed and built inhouse and a diaphragm separator and nonplatinum group catalysts were used as described in detail in the Experimental Section. We used electrodeposited NiMo for the hydrogen evolution reaction and electrodeposited NiFeO_x for the oxygen evolution reaction (OER). In the thermally integrated device, a HE was attached to the back of the PV and the electrolyte was pumped through it before entering the EC stack (scheme in **Figure 1b**). The HE consisted of an aluminum plate (50 cm \times 50 cm), protected from the electrolyte by a thin stainless steel sheet, a ≈ 1.5 mm-thick ethylene propylene diene monomer (EPDM) rubber gasket, and a 1 cm thick polymer (polyoxymethylene, POM) back plate. The gasket formed two distinct flow chambers to keep the anolyte and catholyte circulations separate. The EC stack was bolted to an aluminum profile frame fixed to the back of the HE that carried the weight of the device and acted as the attachment point to the test rig. The PV was clamped to the HE, and we used a graphite laminate

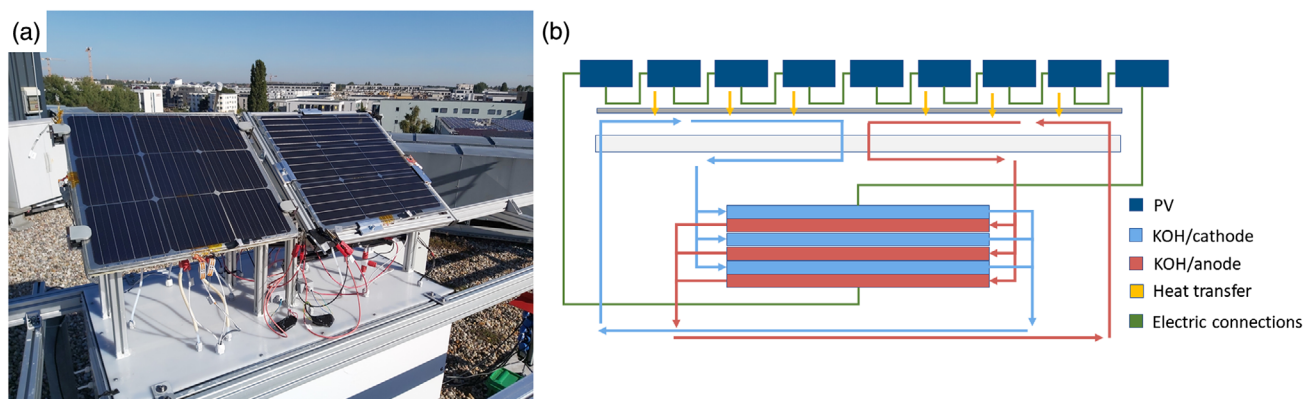


Figure 1. a) The PV EC devices in the rooftop test rig outdoors at HZB, Berlin Adlershof (Germany) and b) the schematic of the electrolyte and heat flow and electric connections in the integrated PV EC, with pumps, etc. excluded. In (a), the device with the HE is on the left. The EC stacks are mostly hidden behind the PV modules, but part of the stack can be seen on the right under the PV without HE.

sheet with stainless steel core (Klinger, Austria) between them to improve the thermal contact. (Thermal grease was also considered, but it was not used as heat transfer, as it was not significantly better than with the steel-graphite sheet and using it for large areas was quite messy.) The electrolyte reservoirs were polytetrafluoroethylene (PTFE) bottles, the electrolyte was continuously pumped in the circulation at a constant rate of $\approx 100 \text{ mL min}^{-1}$, and we did not actively control the electrolyte temperature (e.g., cool, heat, or set a constant temperature).

3. Experimental Section

3.1. Catalyst Deposition

The electrodeposition of $15 \text{ cm} \times 15 \text{ cm}$ NiMo on Ni foam (Nanografi, Turkey) was conducted in a semiautomated coating device (STANDARDWANNE TG 05, Walter Lemmen, Germany) via a two-electrode configuration at room temperature (photograph in Figure S1a, Supporting Information). For better uniformity, two Ni foams with a size of $17 \text{ cm} \times 15 \text{ cm}$ were used as counter electrodes and were placed in parallel on both sides of the working electrode. The working electrode (also $17 \text{ cm} \times 15 \text{ cm}$ Ni foam) was connected to an electrical motor that moved it back and forth to enhance mass transport during deposition. The electrodeposition recipe was adapted from our previous study on electrodeposited NiMo.^[25] The electrodeposition bath composed of 4.5 L deionized (DI) water, 0.030 M $\text{NiSO}_4 \cdot 6\text{H}_2\text{O}$, 0.020 M $\text{Na}_2\text{MoO}_4 \cdot 2\text{H}_2\text{O}$, and 0.030 M $\text{Na}_3\text{C}_6\text{H}_5\text{O}_7$, and the pH of the bath was controlled to be 10.0 with aqueous ammonia. About 35 mL of 20 weight-% ammonia solution was needed for this. The electrodeposition was performed with Parstat 4000 potentiostat (AMETEK Scientific Instruments) as chronopotentiometry at -10 mA cm^{-2} for 300 s.

The electrodeposition of the $15 \text{ cm} \times 15 \text{ cm}$ NiFeO_x on Ni foam was conducted using the same setup that was used for NiMo deposition. The deposition bath composed of 4.5 L DI water, 5.8 g L^{-1} $\text{FeSO}_4 \cdot 7\text{H}_2\text{O}$, 67.5 g L^{-1} NiSO_4 , 0.48 g L^{-1} sodium dodecyl sulfate, 82 mL L^{-1} H_3BO_4 (4%), and 0.26 L^{-1} citric acid, adapted from the recipe used by Thommes et al.^[26] Similarly, like NiMo deposition, NiFeO_x was deposited at -10 mA cm^{-2} DC current for 300 s. After the deposition, the working electrode was rinsed with DI water three times and dried in oven at 60°C .

To characterize the uniformity of the deposited catalysts, smaller samples ($\approx 1 \text{ cm} \times 5 \text{ cm}$) were cut from $15 \text{ cm} \times 15 \text{ cm}$ sized electrodes, limited to $\approx 1 \text{ cm}^2$ active area with nonconductive epoxy (LOCTITE EA 9492) and they were tested in 1.0 M KOH (Sigma Aldrich) at 2 mV s^{-1} scan rate, using a Hg/HgO reference electrode filled with 1.0 M KOH. Measurements of the smaller samples revealed that the catalyst was deposited somewhat non-uniformly (Supporting Information), most likely due to voltage losses in electrolyte and the resulting nonuniform current density distribution.^[27–29] In general, the performance was similar to our previous results of $\approx 1 \text{ cm}^2$ samples of these materials deposited on FTO.^[25,30] As even the worst-performing regions of the electrodes were satisfactory, we continued using the described deposition recipes for the electrodes in the EC stacks.

3.2. Materials and Electrochemical Characterization of the Electrolyzer Stacks

The Ni foam-based electrodes were separated with a Zirfon UTP Perl 500 Plus (AGFA) diaphragm, and the EC cells in the stack were electrically connected to each other with $\approx 1 \text{ cm}$ -wide strips of 0.25 mm-thick Ni foil (Alfa Aesar). In addition, we had 80 threads per inch (TPI) 304 stainless steel mesh (Koenen GmbH) between the Ni foam electrodes and flow field plates made of POM (RS Components), as this seemed to reduce the compression on the Ni foam in the cell. The EC stack was compressed between glass-reinforced Nylon 66 (30% glass, RS Components) end plates with stainless steel bolts or threaded rods. The electrolyte in all EC stacks and PV EC measurements was 1.0 M KOH. The electrolyte volume depended on the measurement, but $\approx 300 \text{ mL}$ of liquid at both the anode and cathode circulation was used when the stacks were measured separately of the PVs.

In total, three electrolyzer stacks were used, all with three electrolysis cells in series and using the same catalysts and separator. The differences were related to the electrolyte tubing. In the first assembled and tested EC stack, the tube manifolding was outside the EC stack, whereas in the later two, the manifold was internal and built in the flow field plates, so only four liquid inlets and outlets in total were needed at the end plates. The only difference between the EC stacks with internal manifold was that the stack used with HE had all its fluid connections at one end plate, and the stack used without HE had the anode connections at one end plate and the cathode connections at the other (see Figure S2, Supporting Information). Placing all connections in one end plate minimized the space needed between the stack and the back of the HE and left the liquid connections accessible also when the PV EC was assembled.

We measured the EC stacks with a FlexP0012 booster controlled by a SP-150 potentiostat (both from BioLogic Sciences Instruments, France). The EC stack characterization protocol was adapted from Bender et al. and the guidelines of the EU harmonized protocol, and the details are shown in the supporting information.^[31,32] It was known to us that the EC stack performance could drop quite rapidly, most likely due to OER catalyst degradation.^[30] Therefore, we included also cyclic voltammetry (CV) and electrochemical impedance spectroscopy (EIS) measurements before the other steps, in between them, and after the last point of the polarization curve measurement to be able to monitor and quantify this.

3.3. PV Modules and Their Electric Characterization

As described in Section 2, we used two similar PV modules, both consisting of nine 6 in. SHJ PV cells (CEA INES, France) connected electrically in series, the total module area being 2600 cm^2 and the area of each cell 244.3 cm^2 . The modules also had two four-wire-connected Pt100 thermometers (TE Connectivity) inside them in small pits drilled to the aluminum back plate, although one of the thermometers in the module used without HE was unfortunately short circuited during module construction, leaving this module with one working thermometer.

We measured the I - V curves of both PV modules before and after the outdoor measurements using an LED simulator (Wavelabs, maximum illuminated area 55 cm × 55 cm, class A spectral match, class B uniformity, 4.8% nonuniformity), calibrated with a silicon reference cell (Fraunhofer ISE, Germany) and the same FlexP0012 booster and SP-150 potentiostat that were used with the EC stacks. In both cases, we determined the effect of irradiance on the performance at room temperature. In the measurements before outdoor tests, we also measured the performance under 1000 W m⁻² at increased temperatures. With the module that was used without HE, we measured the operation at up to about 50 °C, but with the module used with the HE, we could unfortunately measure only up to 40 °C due to technical problems. The temperature dependency was measured under continuous 1000 W m⁻² irradiance with the PV module heating up freely, and the I - V curve was recorded, when the integrated thermometers showed that the module reached a given temperature, for example, 30 °C. For the effect of irradiance on the PV operation, the I - V curve was measured during 5 s-long flashes (single CV at 4 V s⁻¹ sweep rate from +0.1 V vs. open-circuit voltage to -0.1 V and back) and the PV temperature was monitored by the built-in Pt100 thermometers. The same I - V sweep settings were used also at higher temperatures under continuous illumination.

3.4. Indoor Testing of Coupled PV ECs

Before the outdoor measurements, the PV EC operation with and without HE was measured in the same sun simulator that we used for PV characterization under continuous 1000 W m⁻² irradiance. Both the device with and without HE used the same EC stack in all measurements, but the PV module was changed. The measurement was started at room temperature, lasted for one hour under constant 1000 W m⁻² irradiation, and the temperatures, gas flows, and electric current were continuously measured. For the configuration with the HE, we also measured the PV and EC stack voltages. Both indoors and outdoors, we used ≈700 mL of electrolyte (350 mL/side) without the HE and with HE of ≈1200 mL (600 mL/side) due to the additional volume needed to fill the HE. The first results from these measurements have already been reported elsewhere,^[22] and herein we discuss the indoor operation mainly in comparison to the outdoor measurements.

The electrolyte heating power was calculated from the inlet and outlet temperatures of the HE T_{in} and T_{out} , respectively, the electrolyte pumping rate Q , and the specific heat capacity of the electrolyte c_p .

$$P = Q\rho c_p(T_{out} - T_{in}) \quad (1)$$

The electrolyte was aqueous 1.0 M KOH and we used 1059.9 kg m⁻³ density (ρ) and 3993.5 J kg⁻¹ specific heat capacity, corresponding to 5.3 weight percent solution at 25 °C temperature.^[33] Electrolyte pumping rate was 100 mL min⁻¹ at both the anode and the cathode circulation, and the total power was the sum of the power at the anode and cathode sides. This method assumes steady-state operation and in changing operating conditions the outlet temperature corresponds to an earlier inlet temperature that may differ from the one used in this

calculation. The HE volume (up to ≈45 cm × 20 cm × 1.5 mm per side) means that this delay could be about 1–2 min, which roughly matches how long it took for the electrolyte to start exiting the HE after entering it, when filling the system with electrolyte. In addition to the power, we also calculated the thermal conductance from PV to electrolyte. The HE consisted of two separate chambers, one for the cathode and the other for the anode circulation. For one half of the HE, the conductance was simply the heating power (Equation (1)) divided by the temperature difference between the PV and the electrolyte

$$k_{HE} = \frac{P}{T_{PV} - \frac{T_{out} + T_{in}}{2}} = \frac{Q\rho c_p(T_{out} - T_{in})}{T_{PV} - \frac{T_{out} + T_{in}}{2}} \quad (2)$$

Here the PV temperature (T_{PV}) was the temperature measured by the Pt100 at the center of the PV module, as the module used with HE had two thermometers at different locations. In the case of one half, the temperatures naturally refer directly to the measured values, but in the case of the whole HE, the average electrolyte temperature in the denominator is the mean of both inlets and both outlets. The power in the nominator would be the sum of the halves or the temperature difference the sum of outlet temperatures minus the sum of inlet temperatures. The area-normalized conductivity (W (K m²)⁻¹) was then calculated by dividing the conductance by the PV HE contact area ($A_{PV|HE}$), 50 cm × 50 cm, or 25 cm × 50 cm for one half. For one half of the HE

$$\kappa_{HE} = \frac{Q\rho c_p(T_{out} - T_{in})}{A_{PV|HE}(T_{PV} - \frac{T_{out} + T_{in}}{2})} \quad (3)$$

3.5. Outdoor Testing of the PV ECs

The devices were tested outdoors in Berlin, Germany (52° 25' 53.3" N, 13° 31' 25.9" E), tilted 35° up from the horizontal plane and facing south (as Figure 1a shows). The devices were tested simultaneously in outdoor conditions for about 700 h in total, of which the last ≈520 h were continuous, except for few maintenance breaks totaling about 2 h, and they were illuminated and generated hydrogen for about 45% of the time, that is, 310–320 h. Unfortunately, the test had to be ended prematurely due to one of the peristaltic pumps breaking an electrolyte tube, causing a leak. The EC stack that was used in indoor PV EC testing was not used in the outdoor comparison, as both devices had a new EC stack made of the same materials as the stack used indoors, the only differences being their revised and simpler liquid tube connections (Section 3.2 and Figure S2, Supporting Information). In addition to this, we performed a few outdoor measurements with the HE and the EC stack that was used indoors before comparison. In these measurements, the PV was at horizontal tilt and only one device was being measured, that is, a device without HE was not available for comparisons.

We measured the incident irradiance at the tilt plane of the PV modules with a silicon pyranometer (EKO ML-02), the gas flows with mass flow meters (MFMs, Bronkhorst EL-FLOW Select), and electric currents with Hall effect sensors (Iduino ME067) that were calibrated for 0–8 A range with a data recording multimeter (Peak Tech 3430, accuracy 0.8%). As already mentioned,

we measured the PV temperature with Pt100 thermometers integrated inside the modules (between the aluminum plate and the SHJ cells) and the electrolyte temperature with PTFE-protected Pt100 thermometers (4-wire, Bola, Germany). All measurement instruments used indoors and outdoors are listed in Table S3, Supporting Information. With the HE, we measured the temperature at HE inlet, HE outlet/EC stack inlet, and EC stack outlet in both the anode and the cathode circulation (six thermometers) and without HE at the EC stack inlets and outlets (four thermometers). In addition to the electric currents, the voltages of both PV modules and EC stacks were measured, and we also measured the ambient temperature and the temperature inside the instrument enclosure of the test rig (near the MFMs). The system was not pressurized and we verified our irradiance and ambient temperature measurements against the data from an outdoor PV test site near our test rig.

The solar to hydrogen (STH) efficiency (η_{STH}) was evaluated from both the H_2 outflow and the measured electric current. As the name indicates, the MFMs actually measure the mass or molar flow (thermally based on the specific heat capacity and density of the gas^[34]) and convert it to volumetric flow in reference conditions, in our case 20 °C and 1 atm = 1.03125 bar. To calculate the molar flow, we used the densities (ρ) of H_2 and O_2 at 25 °C and 1 atm pressure ($\text{H}_2 = 0.082 \text{ g L}^{-1}$, $\text{O}_2 = 1.308 \text{ g L}^{-1}$ ^[35]) and the ideal gas law to correct for the 5 °C temperature difference.

$$\tilde{n}_i = \frac{Q_i \rho_{i,25}}{M_i} \cdot \frac{298.15 \text{ K}}{293.15 \text{ K}} \quad (4)$$

The volumetric flow given by the MFM is Q_i , the molar mass of the species i is M_i ($\text{H}_2 = 2.001568 \text{ g mol}^{-1}$, $\text{O}_2 = 31.998 \text{ g mol}^{-1}$), and $\rho_{i,25}$ the density at 25 °C and 1 atm. As the pressures in both reference conditions are equal, they cancel each other. The STH efficiency based on the H_2 flow (\tilde{n}_{H_2}) was then

$$\eta_{\text{STH,H}_2} = \frac{\tilde{n}_{\text{H}_2} \Delta G_{\text{H}_2\text{O}}}{A_{\text{PV}} G_{\text{PV}}} = \frac{Q_{\text{H}_2} \rho_{\text{H}_2,25} \Delta G_{\text{H}_2\text{O}}}{M_{\text{H}_2} A_{\text{PV}} G_{\text{PV}}} \cdot \frac{298.15 \text{ K}}{293.15 \text{ K}} \quad (5)$$

The Gibbs free energy ($237.14 \text{ kJ mol}^{-1}$) is $\Delta G_{\text{H}_2\text{O}}$ and the measured irradiance G_{PV} . The PV area (A_{PV}) is the area of the aluminum bottom plate, $51 \text{ cm} \times 51 \text{ cm} = 2601 \text{ cm}^2$. Alternatively, the H_2 flow and the STH efficiency can also be estimated from the electric current (I) using Faraday's law, although this neglects gas crossover, leaks, and other processes that could reduce the amount of storable H_2 and thus correspond to the theoretical maximum of all produced H_2 molecules being successfully stored. The total H_2 production rate corresponds to the electric current multiplied by the number of series-connected ECs in the stack ($N_{\text{EC}} = 3$).

$$\eta_{\text{STH,I}} = \frac{N_{\text{EC}} I \Delta G_{\text{H}_2\text{O}}}{2 F A_{\text{PV}} G_{\text{PV}}} \quad (6)$$

F is the Faraday constant ($96485.332 \text{ C mol}^{-1}$) and 2 is simply the number of electrons needed per one H_2 molecule. The fraction $\frac{\Delta G_{\text{H}_2\text{O}}}{2F}$ is the 1.23 V thermodynamic minimum voltage of water electrolysis (or maximum of H_2 fuel cell).

Faradaic efficiency tells how large fraction of the electric current is in fact converted to useful products, in this case to H_2 that can be stored, that is, flows out through the MFM. In the usual case of only the H_2 flow, the Faradaic efficiency is simply the ratio of the molar flux through the MFM and the electric current (converted to moles/second), which is also equal to the ratio of the STH efficiencies.

$$\eta_{\text{F,H}_2} = \frac{\tilde{n}_{\text{H}_2, \text{MFM}}}{\tilde{n}_{\text{H}_2, \text{I}}} = \frac{\eta_{\text{STH,H}_2}}{\eta_{\text{STH,I}}} = \frac{\frac{Q_{\text{H}_2} \rho_{\text{H}_2,25}}{M_{\text{H}_2}} \cdot \frac{298.15 \text{ K}}{293.15 \text{ K}}}{\frac{N_{\text{EC}} I}{2F}} \quad (7)$$

We calculated this as the fraction of the STH efficiencies, defined in Equation (5) and (6). To supplement this and the gas outflow stoichiometry for EC diagnostics, we also defined the Faradaic efficiency based on the total gas flow as

$$\eta_{\text{F,total}} = \frac{\tilde{n}_{\text{H}_2, \text{MFM}} + \tilde{n}_{\text{O}_2, \text{MFM}}}{1.5 N_{\text{EC}} \tilde{n}_{\text{H}_2, \text{I}}} \quad (8)$$

The multiplier 1.5 for the electric current-based flow or production rate was to adjust it for the theoretical 2:1 H_2 : O_2 stoichiometry. Because of the measurement principle of the MFMs, the molar flow of H_2 crossed over to the anode outstream was seen as O_2 molar flow in almost 1-to-1 ratio and vice versa.^[34] Therefore, any gas crossover without losses due to, for example, leaks or chemical reactions will affect the efficiency based on the H_2 flow but should have only minimal effect on the Faradaic efficiency based on the total gas flow (see Section S5, Supporting Information for details). Therefore, the Faradaic efficiency based on H_2 (i.e., cathode outflow, Equation (7)) tells how large fraction of the generated H_2 can be stored and the total gas outflow-based number (Equation (8)) tells how large fraction of all produced H_2 and O_2 exits the system through either MFM or, inversely, how much of the produced gas is lost to leaks and chemical reactions in the system. The outflow stoichiometry supplements these efficiencies by telling the main or net direction of the gas crossover or the side where losses due to chemical reactions mainly take place (although some of this may already be clear from the differences between the Faradaic efficiencies).

3.6. Error Estimates for the STH Efficiency and the Electrolyte Heating Power

Most of our results are based on the general trends shown by several thousands of data points, so the error margins of a single point are not very significant, and the possible sources of systematic errors during the entire testing period are the most important to us. In addition, each point in our scatter plots (such as Figure 5 in Section 4.3.1) in fact corresponded to the average over several points within a time period, most commonly 1 min, the time resolution of the original measurement being mostly 1 s and even at worst about 5 s. Evaluating the error sources of a single data point still helps with finding the possible sources of systematic errors, so we briefly discuss both in this section, with more details in the Supporting Information.

The relative accuracy of the gas flow was better at higher flows but, in most cases, both the H_2 flow and electric current-based

STH efficiencies had a relative error less than 5%. Because we mainly used the electric currents for the comparison of the relative performance of our devices, and the current sensors were identical and were calibrated simultaneously with the same current passing through both, systematic differences between the measurements of our devices were very unlikely.

In the case of temperatures, it is possible that the PV temperatures were underestimated by a couple of degrees Celsius compared to the liquid and air temperatures, most likely because for PV we had to use different thermometers than for electrolyte and air. Also, one liquid temperature measurement (HE anode-side outlet) probably was faulty, affecting the related data, but otherwise it is unlikely that there are any systematic biases between different temperatures. In the case of the HE power, the width of the error bars of any single point was ≈ 2 W, but the temperature measurements at the cathode side should not have systematic biases compared to each other, so we should be able to trust the general trends of the HE performance. Naturally, the liquid pumping rate and its error had a direct effect on the calculated values ($\approx 5\%$) but, as the rate was kept the same all the time, it could only tilt an already existing pattern in a scatterplot a little.

Degradation over time could naturally affect both the STH efficiency comparison and HE performance and skew the data. However, based on the PV and EC stack measurements before and after the outdoor measurements (Figure 2 and 3, Section 4.1 and 4.2), their performance was not degraded, and the HE showed no obvious signs of changes that would have affected its thermal conductance.

3.7. Infrared Thermography of the PV Modules

On few days we recorded the PV glass surface temperature distribution with an IR camera (FLIR A6700SC), using the manufacturer's software (FLIR ResearchIR, USA) for data analysis and extraction. We used the same procedures that we have used earlier, described by Usamentiaga et al.^[21,36] All thermography recordings were taken directly from the front of the PV modules

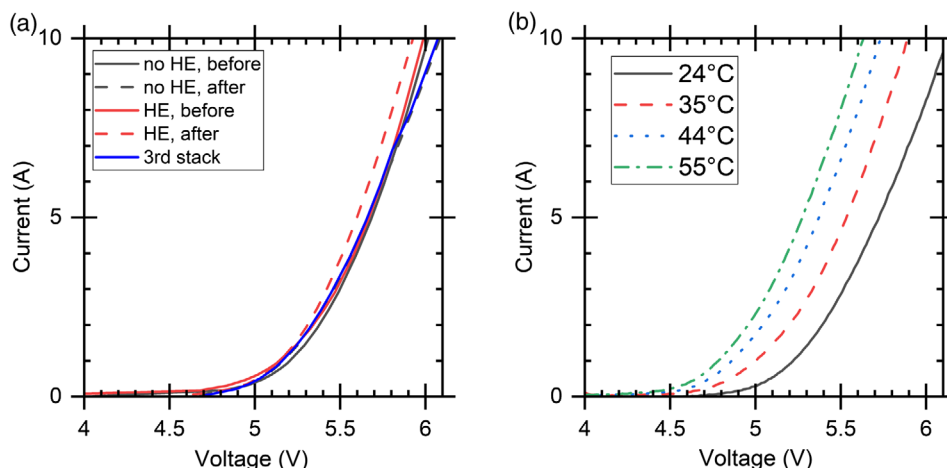


Figure 2. a) I - V curves of the stacks used with and without HE compared to the third stack that we used before the direct comparison and b) the effect of electrolyte temperature on the I - V curve of the third EC stack. With a $15\text{ cm} \times 15\text{ cm}$ geometrical electrode area, the 0–10 A current range corresponds to 0–44 mA cm^{-2} current density range.

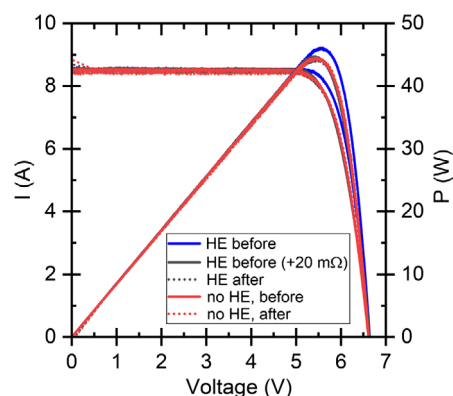


Figure 3. The I - V and power curves of the PV modules under simulated 1000 W m^{-2} irradiance at $25\text{ }^\circ\text{C}$ temperature. The solid and dashed and black and red lines overlap, the solid lines showing the performance before the outdoor measurements and the dashed lines after. The solid blue line shows the original data for the PV module used with the HE and the solid black with $20\text{ m}\Omega$ increased series resistance. The 8.5 A short-circuit current corresponds to 35 mA cm^{-2} current density when normalized to the area of a single PV cell and to 3.3 mA cm^{-2} per PV module area.

when the PV ECs were operating. The camera was at about 1.5 or 3 m distance from the modules (1.5 m, one PV in view; 3 m, both PVs in view) and at about 2 m height from the ground, viewing the PVs at about 50° angle to the surface normal. The temperature distribution in the part of the recording corresponding to the PV was exported as numerical data (a CSV file) for plotting in a different software.

4. Results and Discussion

We begin with the indoor characterization of the EC stacks and the PV modules. Following this, we discuss the operation of the HE, both the heat transfer and its effects on the hydrogen

production rate and on STH efficiency. Finally, we end this section by discussing the PV EC operation outdoors in different weather conditions and in general, and the main results and observations. The HE characterization, of course, is a part of the outdoor PV EC characterization but discussing the components of the PV ECs first should make their comparison easier to understand.

4.1. EC Stack Indoor Performance

We measured the EC stack at room temperature before and after the 700 h outdoor testing. Additionally, we previously measured the effect of temperature on the performance of an EC stack with the same active components, but with slightly different electrolyte inlet and outlet tubing. The results are shown in Figure 2. As all three stacks performed similarly to each other, the temperature very likely affects the two stacks used in the outdoor comparison similarly to the third EC stack. Based on the measurements before and after the outdoor testing, both stacks performed very similarly and, surprisingly, their performance may have improved during testing (mainly $I-V$). Because the stack used with the HE seems to have a slightly lower onset voltage after the outdoor measurements, some iron might have dissolved from the stainless steel sheet of the HE; that was in direct contact with the electrolyte and so could have acted as an iron source, helping to maintain higher catalytic activity than without the HE, similar to what we have observed before with NiFe on FTO.^[30] At over ≈ 1.5 A current, the total gas flow-based Faradaic efficiency (Equation (8)) of all EC stacks is over 97%, except for one measurement that seems to be likely due to gas leaking out (Figure S6, Supporting Information), but there are more differences in the H_2 -based value. Therefore, we think that all EC stacks likely perform at high Faradaic efficiency and the variations in the relative amount of gas exiting from cathode and anode sides may be due to small differences between measurements, possibly including the differences in the inlet and outlet positions. The series resistances of both stacks were increased by about 5 m Ω , increasing the voltage losses at higher currents, but below about 6 A (highest currents that we recorded during the outdoor testing), the net effect for the PV EC operation was a reduction in voltage losses. The increase in series resistance is certainly plausible, but the change is small enough that it might also be within the range of measurement-to-measurement variations. The EC stack performance reduced quickly in the first measurement, as demonstrated by the CVs taken during the measurement (Figure S5, Supporting Information). In the measurements after the outdoor testing, the drop during and after the first CV cycles did not repeat, and in fact CV cycling after other measurement steps yielded slightly better performance than before.

To quantify the effect of electrolyte temperature on the EC stack operation, we determined the voltage for 1, 2, 5, and 10 A currents at different temperatures (Figure S3, Supporting Information). In all cases the linear fit to the values yielded quite similar slopes in the range of -14 to -16 mV $^{\circ}\text{C}^{-1}$, the slope becoming steeper with increasing current. The series resistance of the EC stack was not affected by the temperature and was in the 41–42 m Ω range at all temperatures.

4.2. PV Indoor Performance

Our data indicates that the PV performance was not affected by the outdoor testing and that the modules performed almost identically to each other. After testing, there were practically no differences between the modules, both at 1000 W m^{-2} (Figure 3), as indicated by the overlapping black and red, solid and dashed lines, and at lower irradiances. The maximum power of about 44.5 W corresponds to about 17.1% efficiency per total area or to about 20.2%, if considering only the area of the SHJ cells (244.3 cm² per cell). The average efficiency of the SHJ cells before stringing was 22.3% and their average fill factor 80.3%, which was reduced to 79.1% in the modules. The maximum power point (MPP) voltage decreased by about 15 mV $^{\circ}\text{C}^{-1}$ (Figure S9, Supporting Information), so, in our case, increasing or decreasing the temperature of both the PV and EC by equal amounts might have only small effects on the hydrogen production rate or the STH efficiency. The short-circuit current was about 8.5 A, while on average 9.2 A was measured for single cells in a different (class A) simulator, so we were probably limited by the inhomogeneity of the illumination in our simulator (4.8%, class B, see also Figure S10 and Table S2, Supporting Information). The PV module that was used without HE performed the same before and after outdoor testing. The data from the module used with the HE before outdoor testing indicated somewhat better performance than other measurements, at first sight suggesting degradation during the outdoor measurements. However, as the difference would be explained by about 20 m Ω lower series resistance in the measurement before outdoor testing (contact and/or cables), we consider some small, unintentional difference in electric contacts to be the most likely explanation and not a true difference in PV performance. Therefore, the 5 m Ω difference in the EC stack series resistances could similarly be due to some small difference in measurement connections and not true degradation.

4.3. HE Performance Indoors and Outdoors

4.3.1. Heat Transfer and Its Effect on Hydrogen Production

In the beginning of the indoor measurements, the temperatures were near room temperature and, when the light was turned on, the electric current started instantaneously and gas flows followed with about 5–10 s delay, reaching the maximum flow after 1–2 min; both the current and the gas flows reducing thereafter. The PV temperature without HE reached 75 $^{\circ}\text{C}$ at the end of the measurement (Figure 4), whereas the HE cooled the PV temperature to about 50 $^{\circ}\text{C}$ (Figure S11, Supporting Information). The high temperatures were certainly partly due to poor air circulation (compared to wind outdoors) in the sun simulator, but the benefit of the HE appeared clear. The electrolyte was heated at up to 60 W power, corresponding to circa 23% of the incident irradiance under 1000 W m^{-2} . Without HE the PV temperature was about 20 $^{\circ}\text{C}$ higher (Figure S12, Supporting Information), corresponding to about 300 mV reduction in MPP voltage. This, with the resulting drop in the hydrogen production rate and the STH efficiency, clearly illustrates the effect of increased PV temperature on a PV EC with a PV and an EC that are relatively well

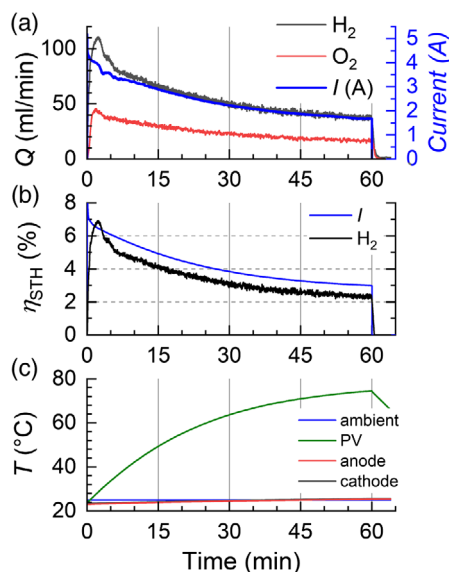


Figure 4. The indoor measurement of PV EC without HE under 1000 W m^{-2} . a) H_2 and O_2 flows and electric current (blue line), b) STH efficiency based on the H_2 flow and the electric current, and c) temperatures. The lines indicating ambient, anode and cathode temperatures overlap each other for most of the measurement. The gas flows and the corresponding STH efficiencies are averaged over 30 s. The other transients are the measured values at 1 s time resolution.

matched at room temperature. This is also the problem that we aimed to solve or at least alleviate, by transferring heat from the PV to the electrolyte.

Figure 5 shows the electrolyte heating (positive power) and cooling power (negative) of the cathode half of the HE as a function of the incident irradiance outdoors (Equation (1)). Figure 5a shows the operation on a few consecutive, almost cloudless, sunny days on 7th–10th October 2021 and Figure 5b all data. This separation allows reducing the number of variables in figure a, showing a clearer pattern and, to some extent, differentiating the effects of clouds etc., and we repeat this treatment in few other figures. Between 400 and 700 W m^{-2} , the vertical height

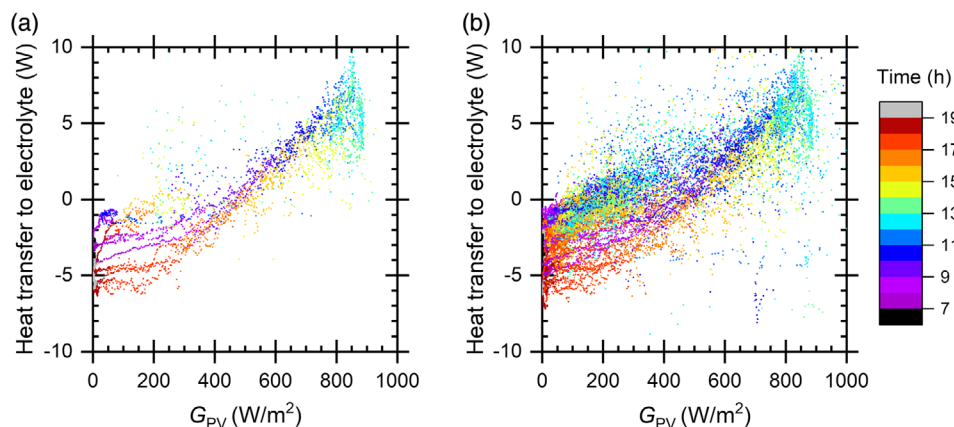


Figure 5. The heat transfer from PV to electrolyte in the cathode circulation during outdoor operation on a) 7th–10th October 2021 in Berlin, Germany and b) all recorded data. There were few, single points at around 800 W m^{-2} and 15 W now shown in (b). The points are averages over 1 min.

of the pattern in Figure 5a is close to the 2 W error bar (Section 3.6 and Supporting Information), but the clear separation of morning and afternoon is almost certainly not due to random or systematic errors, so this is most likely coincidental. Except for the irradiance levels less than 200 W m^{-2} , especially on the sunny days in figure a, the power increases linearly with increasing irradiance. There are a few points around 15 W and 850 W m^{-2} (excluded from the shown range) that seem to be outliers, but otherwise the highest achieved heating power was about 10 W , corresponding to about 9 % of the 850 W m^{-2} irradiance, both numbers clearly lower than what was achieved indoors. Importantly, 0 W , no net heat transfer to either direction, does not occur at night but at a noticeably high 500 W m^{-2} irradiance, and at lower irradiances the HE generally cools the electrolyte by losing heat to the environment, and also increases the PV temperature, opposite to the intended purpose. The PV is warmer than the electrolyte in the HE practically all the time, even when the electrolyte is cooled (Figure S13, Supporting Information), so the cooling must be due to heat being conducted to surrounding air through the polymer back plate. At over 500 W m^{-2} the PV is cooled and the electrolyte heated up, as intended and expected. In the morning, the heating power is higher than in the afternoon or in the evening under the same irradiance, so the heat stored in the electrolyte reduces the PV cooling rate. In addition, on more cloudy days, the heating power at less than 500 W m^{-2} is perhaps a little higher than on the sunny days. At least on the sunny days, neglecting the couple of minutes it takes for the electrolyte to flow from HE inlet to outlet does not change the corresponding temperature difference in a meaningful way, so the negative powers are not due to neglecting this delay in the calculations.

As mentioned earlier in Section 2, the cathode- and anode-side electrolyte circulations were separate also in the HE, both corresponding to half of the contact area with the PV. Most likely due to a problem with the thermometer measuring the anode-side outlet temperature, the outdoor results from the halves differ from each other significantly, the cathode-side temperatures corresponding to physically sensible operation. Indoors, with different Pt100 thermometers, the differences between the two halves were significantly smaller, both heated the electrolyte, and were

thus closer to the outdoor operation of the cathode half, as shown in Figure 5. (The corresponding data of the anode half is in Figure S14, Supporting Information).

The difference between morning and evening and the HE cooling the electrolyte at low irradiances are due to the cyclic operation of the PV EC and electrolyte acting as heat storage. During the day, the increasing irradiance heats up the electrolyte. When the irradiance decreases after the solar noon, at some point the PV and the electrolyte temperatures begin to decrease as the reduced irradiance cannot maintain their temperatures. Heat is still transferred from the PV to the electrolyte, but more is lost to the surrounding air, so the net result is electrolyte being cooled. Therefore, the electrolyte is the main heat carrier of the system that interacts with the environment mostly through the HE and the PV. The PV and electrolyte temperatures follow the irradiance cycle with a delay that depends on their heat capacities and the thermal conductivity of the HE. While it might not be explicit from Figure 5 and S13, Supporting Information, the cyclic operation and resulting heat transfer from electrolyte to air clearly indicate that, at least from the thermal perspective, the PV EC with HE probably never operated at steady state. Regardless of the irradiance, a steady-state, constant irradiance measurement without other power sources is expected to produce a PV temperature that is higher than the electrolyte temperature that in turn is higher than the ambient temperature, as heat should flow from the PV to the electrolyte and to surrounding air. Even with heat escaping from the HE, in steady state, the net electrolyte heating power should be positive when the electrolyte is not heated elsewhere in the system. Without other heat sources, the electrolyte can only lose heat elsewhere in the system through, for example, tubing and reservoir walls, before returning to the HE, and these losses would equal the temperature increase in the HE. Therefore, below about 500 W m^{-2} , the operation is quite certainly not at steady state, and this makes the higher irradiances also questionable in this respect.

Considering the hydrogen production rate, Figure 6 shows the ratio of the measured electric currents as a function of the electrolyte heating power. Ratios larger than one correspond to the device with the HE, generating more hydrogen than the one without. Especially the pattern on the sunny days is very clear, although 0 W does not quite correspond to equal current

densities, but to the PV EC with HE generating a couple of percentage points less hydrogen. The points indicate an almost linear dependence between the heat transfer and the current ratio, with 5 W corresponding to $\approx 4\%$ enhancement. These numbers are likely specific to our device or at least to the types of PV and electrocatalysts, as other materials will respond differently to changes in temperature. Still, due to the clear pattern, it is attractive to entertain the thought that a better HE with the same PV and EC might follow the same curve, but just reaches higher heating power at any irradiance. In this scenario, extrapolating to transferring 25% of the incident irradiance (chosen as approximately equal to the indoor efficiency) under 850 W m^{-2} would correspond to about 28 W in one half of the HE (i.e., almost three times the highest power in Figure 5, and $\approx 55 \text{ W}$ total) and this would lead to about 25–30% increase in the electric current. Using our measured values, a 25% increase would mean increase from $\approx 4.5 \text{ A}$ (and $\approx 7.5\%$ STH) to $\approx 5.6 \text{ A}$ and to $\approx 9.3\%$ STH efficiency. At some point, the short-circuit current and the shape of the PV I - V curve will limit and slow the enhancement but the 25% increase might be possible, based on the expected 7.2 A short-circuit current (at 25°C , Figure S8, Supporting Information). On the other hand, a better HE could also lead to increased PV temperatures in the evenings and mornings, significantly reducing H_2 production rates at low irradiances. Still, the enhancement at high irradiances should provide a net increase in daily H_2 yield, at least on sunny days, even without further developing the rest of the thermal operation of the system.

The HE performance (thermal conductance from PV and insulation from air) and the electrolyte reservoir size, that is, total heat capacity, affect both how fast and how much the electrolyte temperature changes and how much higher the PV temperature can be than the electrolyte temperature. High thermal conductance increases the heating power and reduces the temperature difference between the PV and the electrolyte. A large reservoir size reduces the maximum temperatures and hence the temperature variation over the daily cycle. Still, if the electrolyte is not significantly cooled outside the HE (and PV and EC), the heat transfer to and from the electrolyte will be cyclic and the HE will cool the electrolyte and warm up the PV compared to a nonintegrated PV EC (illustrated with measurement transients in

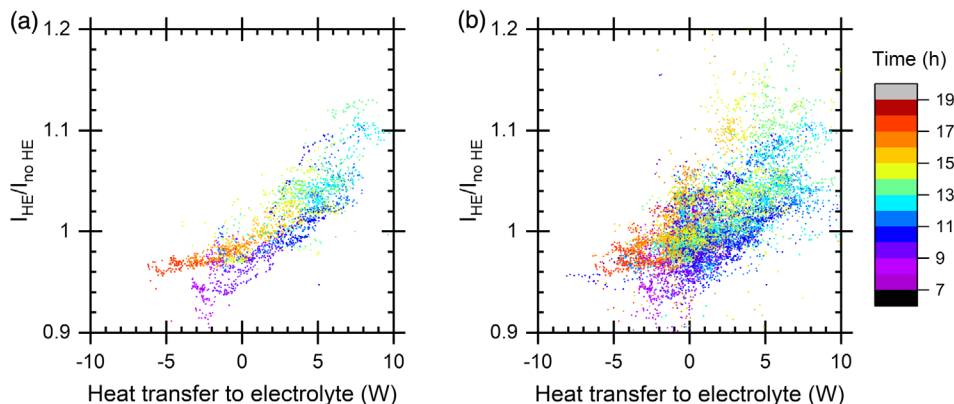


Figure 6. Ratio of the electric currents versus electrolyte heating power in the cathode circulation. a) Sunny days on 7th–10th October and b) all recorded data. The points are averages over 1 min.

Section 4.4.) at relatively high irradiances. A high-performance HE brings the PV and the electrolyte temperatures closer to each other. However, the increased amount of collected heat (higher electrolyte temperature) and efficient dissipation through only the PV (assuming more insulating HE back plate than ours) is likely going to result in a similar cyclic, nonsteady-state operation as in Figure 5, albeit with higher powers and smaller temperature differences between the PV and electrolyte, that is, steeper slope than in Figure S13, Supporting Information. Higher electrolyte temperature will, of course, increase the heat dissipation through the tubes and the reservoir walls but, unless the reservoirs are small (leading to further increased temperatures and heat dissipation) and/or electrolyte cooling is improved, we believe that the cyclic operation remains. After all, the absorbed heat must be dissipated to the surroundings at some time somewhere in the system. If not through a specific cooler, then through the HE and the PV at night and very likely also in early morning and late evening. It is not clear what would happen to the 0 W point, but its irradiance most likely depends also on several environmental factors, such as the length of day versus night, maximum irradiance, and difference in ambient temperatures between day and night, in addition to the system around the PV EC. In summer, with longer days and shorter nights, this irradiance threshold could be higher than in these autumn measurements.

4.3.2. Thermography Images of the PVs

On a few days we recorded the temperature distributions of the PVs using an IR camera. The typical temperature distributions are shown in Figure 7. The images in Figure 7a,b were recorded on 7th October 2021 at 10:55–10:56 (a before b) and the others on 11th October 2021 at 14:25. (The measured transients on these days are shown in Figure 9 and S15, Supporting Information.) Figures at the left side (7a and 7c) correspond to the PV with HE and those on the right side (7b and 7d) without. On 7th October 2021 the weather was sunny and cloudless with $\approx 730 \text{ W m}^{-2}$ irradiance and 17 °C ambient temperature, and on 11th October 2021 mostly sunny and lightly cloudy with $\approx 400 \text{ W m}^{-2}$ irradiance and 15 °C ambient temperature, as the recording was taken during a slightly cloudy period. The reader may, for better comprehension, also refer to the photograph of the setup, corresponding to the thermal images, presented in Figure 1a.

The general patterns of the PV temperature distributions with and without HE differ from each other in few ways. The PV is clamped to the HE from the edges at left and right, which, together with the HE top plate slightly bulging at few points, unfortunately left a small gap at the middle. This can be seen as the elongated, vertical hotspot. The clamping spots are also clearly distinguishable in Figure 7c as cold spots at the left and right edges of the PV. Without the HE, the warmest area is wider and its location and shape are perhaps a little more affected by the wind than with the HE. The shape of the hotspot in Figure 7a,c together with the information about the gap illustrates the main problem of the HE: in-plane heat transport is needed, in addition to through-plane transport, making the path from PV to electrolyte longer than ideal and reducing the thermal conductance. Although we enhanced the PV EC operation with

the HE, further improvements should be possible simply by optimizing the structural and mechanical details to make the aluminum plates of the HE and the PV flatter. A good contact between the HE and PV should result in a more uniform temperature distribution with less pronounced hotspots.

Comparing the temperature differences between the thermal images with and without HE to Figure 5 (depicting variation of heat transfer with irradiance and time of the day), the cooling effect of the HE in sunny conditions and the lack of it in more cloudy weather are clear. However, on 11th October 2021, the left half of both PVs is cooler, whereas on 7th October 2021, the temperature distributions are more symmetric. This difference is most likely due to wind speeds and a slightly different wind direction. On 7th October 2021, the wind was 0.6 m s^{-1} from southwest and on 11th October 2021 3.5 m s^{-1} from west, that is, left to right in Figure 7. As the left and right half of the recordings with HE, especially in a), are not very different from each other, the anode and cathode halves of the HE probably operated approximately equally well. In the recordings the anode-side circulation is the left half and cathode the right, so the slightly less-efficient anode-side electrolyte heating could perhaps be explained by the wind direction and cooler PV temperature seen in Figure 7, but the difference between Figure 5 and S13, Supporting Information, is quite large to be caused by the wind alone.

4.4. Outdoor PV EC Hydrogen Generation Performance

The PV ECs with and without HE were operated simultaneously in outdoor conditions, the longest period of continuous operation being about 500 h, preceded by three shorter tests that together amount to ≈ 200 additional hours of operation (Figure 8). Similarly to the indoor measurements, after connecting PVs and EC stacks at the beginning of a measurement, electric current started instantaneously and gas flows followed with a short, few seconds delay. Some main features can be seen already from a quick inspection of the data: 1) The H_2 flow and electric current transients follow the irradiance transient, demonstrating that the device operation is powered by sunlight. 2) On sunny days (7th–10th October 2021), the STH efficiency is lowest at noon with highest irradiance and increases as irradiance decreases. 3) The performance with and without the HE is generally quite similar, mostly 8–12% STH efficiency with the H_2 flow rate peaks at around 120 mL min^{-1} per system. However, the peak electric currents are visibly higher with the HE, corresponding to higher STH efficiency under high irradiance. 4) The STH efficiencies based on the H_2 flow and electric current are similar to each other, indicating a high Faradaic efficiency.

In comparison to the 8–12% STH efficiency range in the outdoor measurements, the indoor characterization under 1000 W m^{-2} yielded about 2–3% without HE and 6–6.5% with HE after 1 h of continuous operation (Figure 4 and S10, Supporting Information). As discussed earlier, indoors, the PV with HE was about 20 °C cooler at the end of 1 h measurement (Figure S11, Supporting Information) and the efficiencies being lower than outdoors were certainly at least in part due to more constricted air circulation causing higher PV temperatures.

Based on the recorded electric currents and the EC stack voltages, the stacks operated generally as expected from the indoor

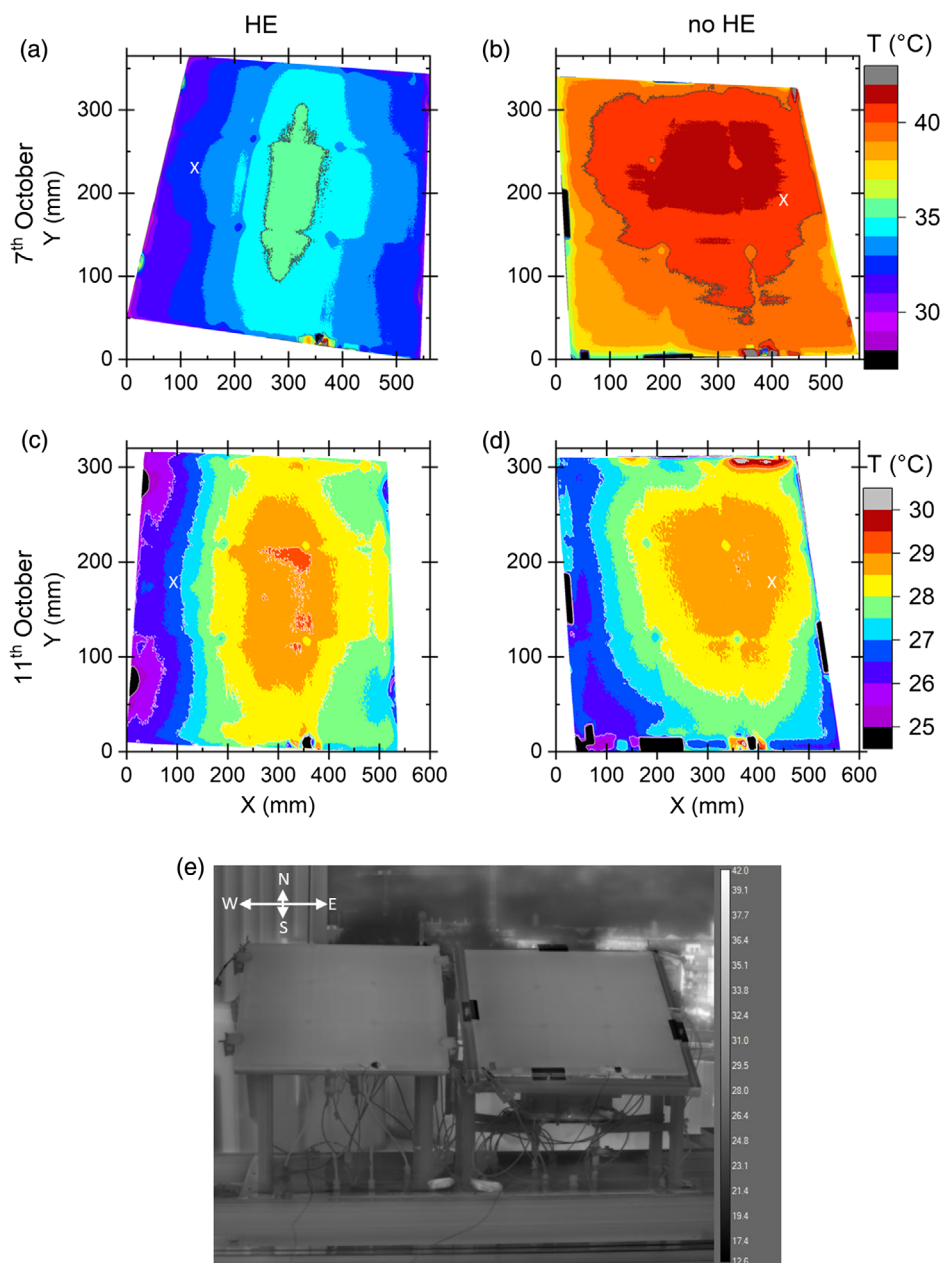


Figure 7. Thermography recordings of the PV EC a,c) with HE and b,d) without it on 7th October 2021 (a,b) and on 11th October 2021 (c,d), and e) the greyscale image from which (c) and (d) were extracted. Both rows have a common temperature scale, that is, a & b and c & d. Due to PV tilt and perspective, the Y axis does not correspond to the true size of the PV module, but is given as a frame of reference. In all cases, the figures were scaled so that the width of the PV at its middle height ($Y \approx 150$ mm) is 510 mm. The cardinal directions, with the camera pointing to north and PVs facing south, are added to Figure (e). The white “X”s in Figure (a–d) indicate the approximate location of the PV temperature measurement.

measurements. The EC stack used with the HE achieved higher maximum temperatures and consequently lower operating voltages and the effect of temperature on its performance appears clearer (Figure S16, Supporting Information). Considering the temperature and its effect, the EC stack operated at a lower voltage than expected and the effect of the (electrolyte) temperature was smaller than indoors. The reason for this is not known to us.

The faradaic efficiency based on the H_2 outflow was generally over 90%, without HE almost constant around 94% and with HE

increasing with current from about 90% to 98% (Figure S17, Supporting Information). Considering the total gas outflow, the effect of the electric current was reduced, indicating H_2 crossing to the anode side, especially at low currents in the PV EC with HE. This is also clear from the outflow ratios (Figure S18, Supporting Information), whose irradiance or current dependencies differ from each other. The total outflow-based Faradaic efficiency of the device with the HE was about 5 percentage points higher over the entire current range, which might be, for

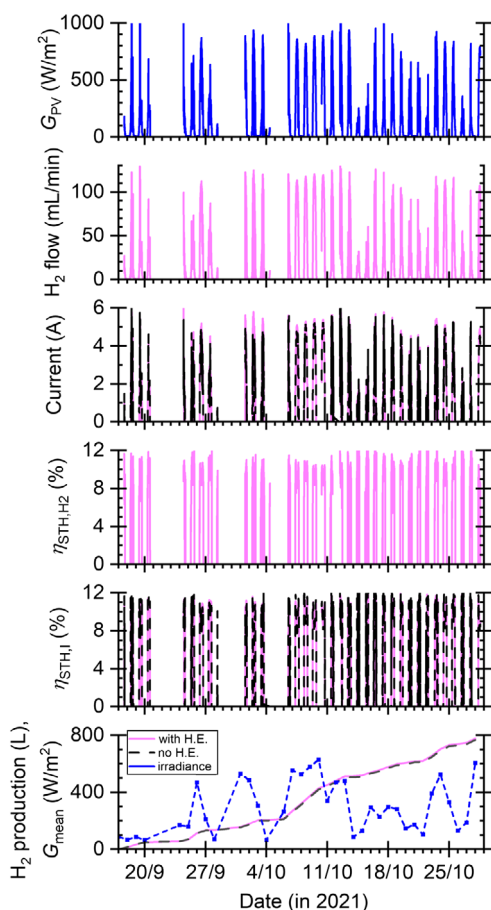


Figure 8. PV EC comparison testing: irradiance, measured H₂ flow (with H.E.), electric current, STH efficiency based on H₂ flow and electric current, and cumulative H₂ production and daily mean irradiance. The date ticks correspond to the beginning of the date at midnight and the legend is valid for all graphs in the figure.

example, due to the different EC stack tilt increasing gas cross-over and recombination (electrodes horizontal without HE vs. at 35° tilt with) or simply some unfortunate leak in the system without HE. The EC stacks should be nearly identical so, at least in principle, some part of the higher Faradaic efficiency of the thermally integrated device could be due to differences related to the system, the HE, or other small differences in liquid reservoirs and tubing. The different tilt is a clear possible reason for the different current dependencies of H₂-based Faradaic efficiency and gas outflow ratio. At over $\approx 500 \text{ W m}^{-2}$, both ECs produced gases at about 2:1 ratio, but in both cases the mean seems to be a little higher than 2.0. This could be due to O₂ being lost to leaks or reactions or crossing over from the anode to the cathode side due to, for example, electro-osmosis.^[37] Despite the differences, the Faradaic efficiencies are not totally different, so using the electric current for efficiency comparison instead of the hydrogen flow should not skew our comparison. There were few points indicating over 100% faradaic efficiency (Figure S17, Supporting Information), but, considering their rarity, they were probably results of irradiance reduction and the delay in gas flow compared to the electric current.

Over the time period in Figure 8, both devices produced about 800 L of H₂ at 20 °C and 1 atm, estimated from electric current. The H₂ flow of the PV EC with HE yielded 814 L in the same conditions. The higher yield is due to the electric current being underestimated as 0 A, when it was less than ≈ 1 A. For the most representative comparison, to avoid biasing it to either direction, we consider electric current only at the times when nonzero electric current was recorded for both devices, which yields 770 L total production without HE and 780 L with HE, about 10 L increase in the cumulative total H₂ production (Figure 8, bottom). Compared to about 13% annual enhancement in a (steady-state) simulation study, this is a very modest increase, but an increase nonetheless.^[23]

Unfortunately for the cumulative production comparisons, we had problems with recording the gas outflows of the device without HE, so we do not have this data for all times when the devices operated. The electric currents were recorded reliably (as Figure 8 shows), so we use them instead. However, as mentioned, the electric currents were falsely recorded as 0 A when less than about 1 A, which, in practice, means that we can compare the hydrogen production rate of the devices at over $\approx 150 \text{ W m}^{-2}$ irradiances but not below this limit. There were few short intervals when data was not recorded, but we have the direct comparison of the device temperatures and electric currents for almost the entirety of the measurement period.

Following this general outlook on the PV EC operation, we consider the device operation on three different days (sunny, varying cloudy, and very cloudy), before taking a more detailed look into the effects of irradiance and temperature.

4.4.1. Operation on a Sunny Day

We consider 7th October 2021 as an example of a sunny day. The measured irradiance, electric current, STH efficiency, and temperatures are shown in Figure 9. All transients are averaged over 10 s. Except for the sharp dip soon after 15:00, the rest of the day was sunny with almost no quick changes in the irradiance. The same general shape is seen in the current transients. The current and the STH efficiency show the two main effects of the HE. First, in the morning, the device with HE produces less H₂ due to lower (!) EC temperature. Between 9:00 and 9:30, the temperature differences become negligible and soon after both devices operate at the same efficiency and temperature. From this point on, until about 16:00, the HE increases the EC temperature and the H₂ production rate. Generally, the PV temperature with the HE was lower than without, as already illustrated in Figure 7a,b. Wind speed and direction also affected this. The most common wind direction during our testing was from between south and west, and this was the case for most of the day on 7th October (Figure S19, Supporting Information). However, soon after 12:00, the wind turned to northeast, almost directly against the backs of the PVs, and this was the direction also on 8th October for the entire day. With wind from behind the PV ECs, the PV temperatures were very similar to each other already in the afternoon of 7th October, although the PV with HE exhibited fewer and smaller quick changes. The wind speed on 8th October was higher than on 7th, lowering both PV temperatures. However, the main difference to most other days was the

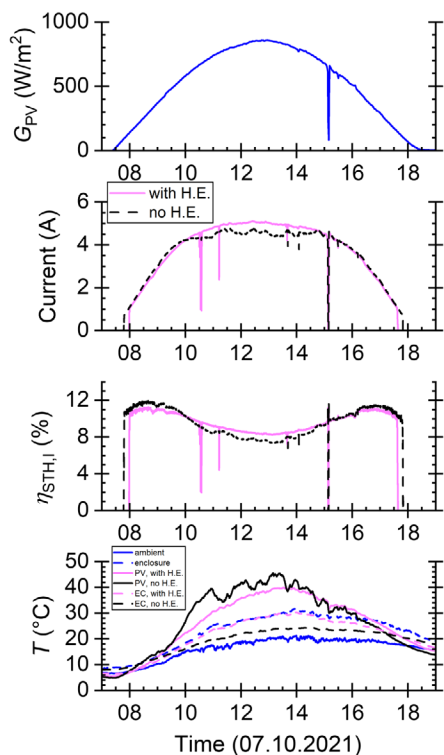


Figure 9. PV EC operation on a sunny clear day, 7th October 2021 in Berlin, Germany: Transients for irradiance, electric currents, STH efficiencies, and temperatures compared for situation with or without thermal integration using a HE. The thermography recordings in Figure 7a,b were taken at 10:55–10:56.

wind direction and the PV without HE was a little cooler than the PV with the HE (Figure S20, Supporting Information). This also demonstrated that the heat transfer through the aluminum bottom plate was faster than through the top glass, as the PV without HE was warmer than the PV with HE when wind was mostly against the top glass cover. Moreover, considering the wind speed and PV temperatures, the operation on 8th October offers also a convenient alternative way of quantifying the cooling effect of the HE: the PV temperatures were equal, when the wind was about $2\text{--}4\text{ m s}^{-1}$ against the aluminum back plate.

The highest STH efficiencies ($\approx 11\text{--}12\%$) occurred in the morning and in the evening under less than 300 W m^{-2} irradiance and the minimum corresponded to the maximum irradiance and the maximum H_2 generation rate. The minimum efficiency values in this case were about 9% with the HE and about 8% without, and the H_2 generation rates ($4.4\text{--}5.1\text{ A}$ and $100\text{--}110\text{ mL min}^{-1}$) corresponded to about $16\text{--}19\text{ W}$ power. The HE reduces the amplitude of small variations in H_2 production during the day but makes the general shape of the H_2 production a little narrower and sharper, meaning generally slightly longer ramp-up and -down phases, or/and higher rates in the morning and in the evening, as hinted by Figure 5 and 6. In the evening, the PV temperature with HE was higher than without it and, in the case of the EC stack temperature, the opposite occurred simultaneously, so with the HE, the electrolyte cooling must have been faster while the PV cooling was reduced. Increased electrolyte temperature, leading to the stored heat

being transferred to air (negative powers in Figure 5, 6 and S13, Supporting Information) while reducing the PV cooling, would explain both. For some time, the EC stack temperature was even slightly higher than the PV temperature (also seen in Figure S13, Supporting Information), although, this might be due to a small offset in PV temperature compared to the other temperatures.

Both in Figure 9 and in other transients the PV temperatures at night were a couple degrees colder than the ambient temperature, most likely due to some error in the PV temperature. Our ambient temperature measurement matched the data from the weather station well, although at night it was a little cooler, and during day slightly warmer, most likely due to the closeness of the PV EC and the instrument enclosure. Considering that the previous comparison of PV temperatures to the IR camera images (Section 4.3.2 and Table S4, Supporting Information) showed the Pt100 data to be similarly $2\text{--}3\text{ }^\circ\text{C}$ cooler than the IR images, this could be a roughly constant offset underestimating both PV temperatures by a couple degrees.

Very typically, also on this day, the temperature of the EC stack of the thermally integrated device was about equal to or higher than the temperature of the air in the equipment enclosure, where also the electrolyte reservoirs were located, whereas the EC stack without HE was almost always cooler than the enclosure (see also Figure 10 and 11). Depending on the operating current density, size, and materials (e.g., thermal conductivity), the EC stacks could also heat up the electrolyte but, in our case,

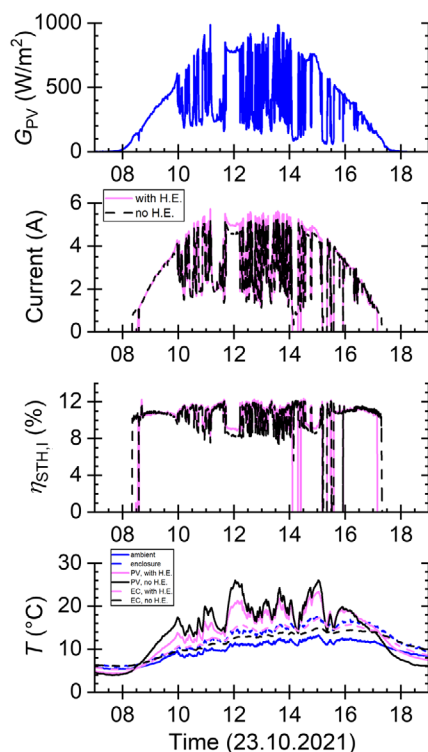


Figure 10. Irradiance, hydrogen production rate, solar-to-hydrogen efficiency, as well as device, ambient, and enclosure temperature during the PV EC operation on 23rd October 2021 in Berlin, Germany, with fluctuating weather conditions.

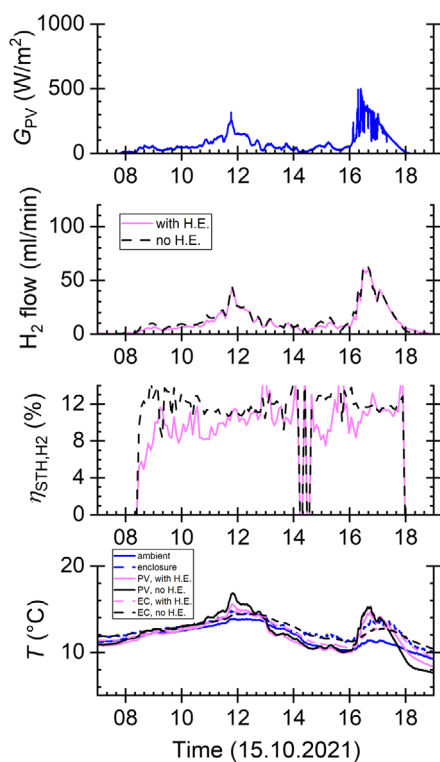


Figure 11. Irradiance, hydrogen production rate, solar-to-hydrogen efficiency, as well as device, ambient, and enclosure temperature during PV EC operation on a cloudy day, 15th October 2021 in Berlin, Germany, with very cloudy weather conditions.

electrolyte was slightly cooled in both EC stacks. Therefore, without the HE, the electrolyte was not heated up outside the enclosure so its temperature increase over the day and the difference to the ambient temperature were most likely due to the enclosure temperature (sun, warm KOH in the system with HE, and heat from electric equipment, etc. increasing the temperature). In the case of the HE, heat may have been conducted from liquid to air (possibly causing the nearly equal temperatures) or vice versa, but the electrolyte heating effect is probably at most the few degrees difference between the EC without HE and the ambient temperature, and the electrolyte temperature measurements nevertheless indicate that heat is transferred from the PV to the electrolyte in sunny conditions.

4.4.2. Operation on a Varyingly Cloudy Day

For an example of operation in fluctuating weather conditions, we select 23rd October 2021 (Figure 10), the day with the largest number of rapid irradiance changes (188 over 10% per 10 s increases, see Figure S21, Supporting Information), calculated using the approach reported elsewhere.^[38] Although we did not observe noticeable EC stack degradation, this would, in principle, make it the day that would degrade the EC stack the most during our measurement period. The morning begins sunny and, at first, the irradiance and hydrogen transients are similar to the sunny day but between 10:00 and 16:00 the rapid irradiance changes increase and reduce the electric current (hydrogen

production rate). Most peaks and dips are short but there are a few longer ones at about 11:00 to 13:00 and at 14:00 to 15:00. The sunny morning still allows the HE to heat up the electrolyte and cool the PV temperature, compared to the PV without HE.

When compared to the operation on a sunny day, although the irradiance reaches high enough levels that there are clear differences in EC stack and PV temperature and hydrogen production rate, the low irradiance periods and lower ambient temperature reduced the PV temperatures and their difference to the ambient temperature. The wind speeds in the morning are higher than on 7th October, but by noon they are at a similar level. The benefit of the HE is clear in the higher peak currents, but under lower irradiances the STH efficiencies are very similar. Especially in the evening the adverse effect of the HE on the PV and EC temperatures is a little easier to see than in Figure 9.

4.4.3. Operation on a Very Cloudy Day

Our example of a very cloudy day is 15th October 2021 (Figure 11). For most of the day, the incident irradiance was below 200, and 400 $W m^{-2}$ was exceeded only briefly in the early evening. As a difference to the other two days that we presented, the thermally integrated device clearly produced less H_2 than the device without HE. We believe this to be simply because the irradiance was never high enough to warm up the PV and thus the electrolyte, so the morning state persisted for the entire day, except for a short period of time between 16:00 and 17:00 when the irradiance peak increased the PV and EC temperatures. In contrast, the STH efficiencies are higher than on the other two days, but because the total hydrogen production is only about 10% of the production on a sunny day (≈ 5 L vs. ≈ 50 L), this is not really an important detail. Unfortunately, for reasons independent of us, we do not have the data about the wind conditions on this day (speed and direction).

4.4.4. Effect of Irradiance and Temperature

Considering the effect of the HE on the PV EC operation more generally and in more details, we begin with the daily H_2 yield and mean irradiance, shown in Figure 12. At mean irradiance less than about 350 $W m^{-2}$, the device without HE performs

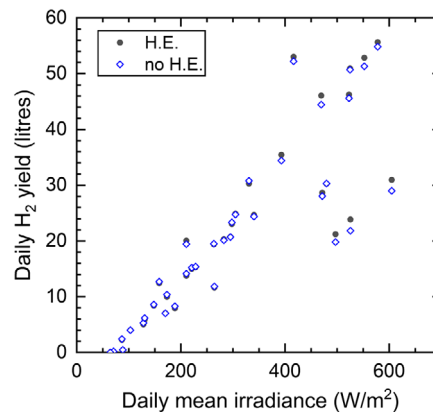


Figure 12. The daily H_2 yields (electric current) with and without HE as a function of the mean irradiance.

as well as the one with HE or slightly better (and there were more low-irradiance days than sunny days during our testing). Conversely, at more than 400 W m^{-2} mean irradiance, the HE increases the H_2 yield. The unusually low H_2 yields at high mean irradiances (about 30 L or less) are due to recorded data not including the entire day, that is, missing morning or evening. Excluding low-irradiance periods both increases the average irradiance and reduces the daily total production by neglecting a productive period. The average irradiances and H_2 yields of the three earlier example days were on 7th October 552 W m^{-2} and $\approx 50 \text{ L}$ (52.4 L with and 50.9 without HE); on 23rd October, 393 W m^{-2} and $\approx 35 \text{ L}$ (35.2 L with and 34.1 L without); and on 15th October 2021, 128 W m^{-2} and $\approx 5 \text{ L}$ (5.0 L with and 5.2 L without).

Figure 13 shows the STH efficiencies calculated from the electric current as a function of the irradiance. There are only few differences between the two devices, both achieve 11–12% efficiency at below 400 W m^{-2} , and at higher irradiances the trend clearly decreases with increasing irradiance. At over 900 W m^{-2} , the most frequent efficiency with HE was about 8.5%, whereas without HE the distribution was wider with the peak just below 8% (Figure S23a, Supporting Information). A second general difference is the effect of increasing ambient temperature: without HE, the points at over 20°C ambient temperature differ from the

lower temperatures more than with the HE, that is, the yellow, orange, and red points are not overlapping with the blue ones and there is more scatter in the graph at all irradiances. To illustrate, the distributions for few irradiance ranges are shown in Figure S23b–d, Supporting Information. The distributions without HE are broader, and the peaks with HE are clearly sharper. At lower irradiances, the peak with HE is at a little lower STH efficiency, but at $650\text{--}750 \text{ W m}^{-2}$ the distribution with HE is at generally higher STH efficiencies, although the most frequent STH efficiencies are equal. The temperature effect in Figure 13 could correspond to the difference in operation in the morning versus in the afternoon after warming up, as the highest ambient temperatures also occur in the afternoon, on sunny days at 14:00–16:00. The STH efficiency was largely insensitive to changes in the ambient, PV, and EC temperatures, the only exception being the clear reduction of the STH efficiency without HE with increasing PV temperature (Figure S24, Supporting Information).

Considering the simultaneous operation (and combining Figure 5 and 6), **Figure 14** shows the relative performance benefit of the HE against the incident irradiance. Figure 14a shows the data from a period of consecutive, almost cloudless sunny days on 7th–10th October 2021, and Figure 14b shows all recorded

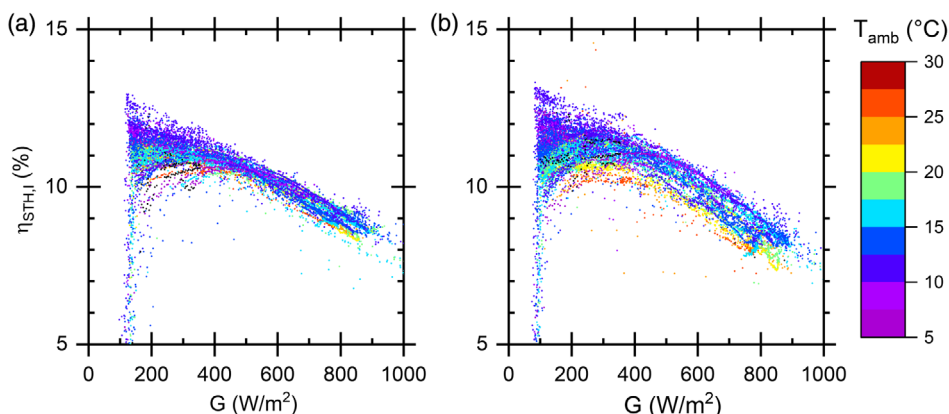


Figure 13. The STH efficiencies based on the electric current with a) HE and b) without it. The values are averages over 1 min.

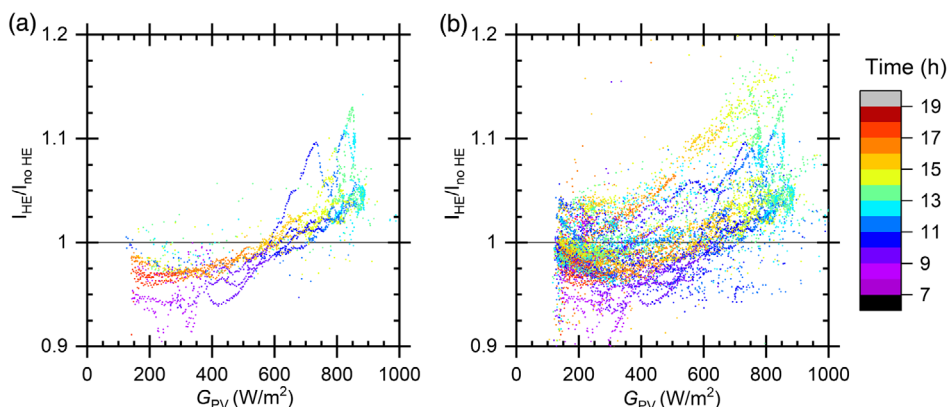


Figure 14. The ratio of the measured electric currents as a function of the irradiance at 60 s averaging time period, a) on 7th–11th October and b) all recorded data. The horizontal line corresponds to ratio of 1, and values higher than that correspond to the HE enhancing the device performance. The color scale indicates the clock time.

data. Generally, the HE enhanced the performance at over $\approx 500 \text{ W m}^{-2}$, although on the sunny days this limit is at about 600 W m^{-2} which matches Figure 9 (and Figure S20, Supporting Information), and the relative differences were mostly less than 5%, although up to 15% was observed. The time reveals the previously described pattern: In the morning, the device with HE performed worse than without it, around noon the HE increased the STH efficiency, and in the afternoon the ratio was higher than before noon at the same irradiance, but the performance with HE was still worse than without HE at low irradiances. The highest ratios in Figure 14a at about 1.1. and at 700 and 850 W m^{-2} were most likely due to the wind speed being lower than at almost all other measurement points (not shown), which would have increased the PV temperature of the device without HE, reducing its performance.

The data in Figure 14a does not contain all (mostly) sunny days during the testing period, as is evident from the other points reaching up to 850 W m^{-2} , but it demonstrates what could be called a base pattern when sunny, cloudless days follow each other. Comparison of Figure 14a,b to each other shows that in more cloudy conditions, the PV EC with the HE performs better at less than 500 W m^{-2} than on cloudless days. This is clearest with the low-irradiance conditions near noon. This effect is due to the varying and cyclic operation of the devices and the amount of heat stored in the electrolyte, discussed in Section 4.3.1. For the annual total production, reduced efficiency at low irradiances is at least a minor problem, which is probably not helped by the slightly increased rates of ramping up and down. Nevertheless, the efficiency is increased the most when the hydrogen production rate is the highest and, despite the larger number of cloudy days, the device with the HE did produce more hydrogen, so the thermal integration was certainly beneficial. However, as discussed with the details of the HE operation, the cyclic and changing operating conditions mean that more than just the HE alone may be needed to maximize the total hydrogen production over longer times.

At the first glance, Figure 14 might appear to contradict literature that indicates that the thermal integration should increase hydrogen production around the year, meaning also in generally low-irradiance conditions (and perhaps especially in such conditions).^[23] However, the crucial differences are that Figure 14 shows the daily operating cycle(s), whereas the simulated yields are cumulative totals over the calendar months based on a steady-state model, but in our case Figure 5 and 6 indicate nonsteady-state operation. It could still be possible to achieve reasonably accurate hydrogen yield predictions with steady-state models, but they would miss the behavior shown in these figures and could consequently overestimate the benefit of thermal integration. The simulated device also had some differences compared to our device that could affect the device dynamics, such as the DC–DC converter and slightly different way of connecting the EC to the heated electrolyte, so the comparisons might not be fully accurate even with a dynamic model.

4.5. Summary of Results and Observations

During our 700 h outdoor testing, we achieved about 8–12% STH efficiency and up to 120 mL min^{-1} hydrogen production rate

with a high Faradaic efficiency, which in the case of the unintegrated device may have suffered from the horizontal electrode tilt. This tilt was simply due to it being the most convenient way of fixing the EC stack to the test rig, so that should be changed if a different tilt improves the Faradaic efficiency. Not unexpectedly, increasing irradiance reduced the STH efficiency, but the ambient temperature had only a minor effect, although the PV EC without HE was clearly more sensitive to, for example, ambient temperature and wind conditions than the integrated device. At over 500 W m^{-2} , the HE increased the H_2 production by up to 5% (up to 10% in rare cases). However, below this threshold, the H_2 production rate was reduced due to the heat stored in the electrolyte maintaining higher PV temperature from evening to morning, and the electrolyte was cooled due to heat escaping through the polymer back plate of the HE. Especially during consecutive sunny days, the thermal operation of the integrated PV EC was clearly cyclic and nonsteady state. On more cloudy days, the HE seems to enhance the operation at lower irradiances than on sunny days, so a better HE increasing the annual net hydrogen production seems probable.

A better HE should further enhance the operation at high irradiance conditions, but, due to the cyclic operation and electrolyte acting as heat storage, in the morning and in evening, the PV could be warmer and the STH efficiency might be even further reduced compared to the results presented here. Therefore, an improved HE might not change the cyclic operation significantly, but could just make the slope of the heating power versus irradiance pattern (Figure 5) steeper. This is not to discourage the use of thermal coupling of PVs and ECs; after all we achieved higher cumulative hydrogen production with the PV EC using the HE in autumn. However, the optimization of its use clearly is not a simple case of only constructing a better component for the device (although this helps). Extracting the most benefits from the thermal coupling likely requires additional ways to control the electrolyte temperature, such as controlling the device operation and heat transfer rate with the electrolyte pumping rate^[17,39] or adding components to the system that improve the electrolyte cooling in the daytime.

The STH efficiencies and device temperatures from indoor testing were clearly lower than during the outdoor testing, even considering the irradiance differences, which are mostly due to the more constricted air flow indoors. The information gained from steady-state indoor testing is naturally useful for general performance-level quantification; the results may be mostly applicable for the PV EC operation around noon on a sunny day, and the thermal conductivity (Equation (3)) and similar quantities can be useful in the correct context. Otherwise, the steady-state temperatures, heat transfer, and performance of the devices are unlikely to accurately reflect the transient operation in outdoor conditions for a large fraction of time. From indoor measurements, the HE conductivity was around $25 \text{ W (K m}^2)^{-1}$, and the outdoor data with stronger air cooling effect (reduced net electrolyte heating power) yielded about $11 \text{ W (K m}^2)^{-1}$ so, unfortunately, even this quantity might not necessarily allow easy comparisons between indoor and outdoor conditions. Based on this thermal conductivity, and on the IR images, the heat transfer was suboptimal, but the HE still

reduced the PV temperature and increased hydrogen production in sunny conditions.

5. Conclusion

PV EC performance can be enhanced with thermal integration, and even relatively modest heat transfer rates produce noticeable differences in hydrogen production rate. In our case, the STH efficiency was increased from about 8% to about 9% at $\approx 800 \text{ W m}^{-2}$ and from a little less than 8% to 8.5% at over 900 W m^{-2} irradiance, and the highest hydrogen production rates were about 120 mL min^{-1} . Somewhat surprisingly, the thermal coupling also reduced the PV EC performance under irradiances less than $\approx 500 \text{ W m}^{-2}$, which was due to the transient and cyclic nature of solar energy, electrolyte acting as a heat storage, and comparatively slow heat transport and dissipation. Improving the HE is expected to enhance the performance under high irradiances, but the cyclic operation could remain and the performance in morning and in evening might even be reduced, meaning that changes to other parts of the system (than the PV EC) may be needed to gain the full benefits of thermal integration. The electrolyte being cooled in the HE under moderately high irradiance also means that steady-state measurements of PV EC operation can be misleading, when considering outdoor operation. Based on both PV modules being at the same temperature on a sunny day with rare wind direction, the cooling effect of HE corresponded to about $2\text{--}4 \text{ m s}^{-1}$ wind against the aluminum back plate. Wind and changing wind conditions outdoors and stagnant air indoors can cause significant differences in device temperatures, hence in their general performance. In our case, compared to outdoor operation, the performance of the device without HE was underestimated, and the heat transferred to electrolyte overestimated. Unfortunately, realistically slow irradiance cycling may be very impractical to realize for indoor testing, so some other alternative methods may have to be developed.

Supporting Information

Supporting Information is available from the Wiley Online Library or from the author.

Acknowledgements

The authors gratefully acknowledge financial support for the PECSYS project, which has received funding from the Fuel Cells and Hydrogen 2 Joint Undertaking under grant agreement no. 735 218. This joint undertaking received support from the European Union's Horizon 2020 Research and Innovation programme and Hydrogen Europe and N.ERGHY. The project started on January 1, 2017, with a duration of 48 months. The authors also acknowledge the support from the German Federal Ministry of Education and Research (BMBF) in the framework of the project CatLab (03EW0015A). AGFA NV is gratefully acknowledged for providing the Zirfon separation membranes used to realize the PV EC devices. C. Ulbrich, M. Riedel, and M. Khenkin of the Outdoor Performance Analysis Group at Helmholtz-Zentrum Berlin are thanked for advice on outdoor device monitoring and access to the measured weather data.

Open Access funding enabled and organized by Projekt DEAL.

Conflict of Interest

The authors declare no conflict of interest.

Author Contributions

S.C. and R.S. took care of conceptualization. E.K. took care of data curation. E.K. took care of formal analysis. R.S., S.C., and B.S. took care of funding acquisition. E.K., R.B., C.S., F.B., and I.D. took care of investigation. E.K. took care of methodology. R.B., C.S., S.J., Q.E., B.S., F.B., I.D. took care of resources. C.S. took care of software. S.C. and B.S. took care of supervision. E.K. took care of writing the original draft and revised manuscript.

Data Availability Statement

The data that support the findings of this study are available from the corresponding author upon reasonable request.

Keywords

electrolyzers, heat transfer, outdoor characterizations, photovoltaics, solar water splitting, thermal integration

Received: September 15, 2022
Published online: December 25, 2022

- [1] IEA (2021), *Key World Energy Statistics*, OECD Publishing, Paris **2021**, <https://doi.org/10.1787/2ef8cebc-en>.
- [2] M. Aneke, M. Wang, *Appl. Energy* **2016**, *179*, 350.
- [3] N. Armaroli, V. Balzani, *Chem. - Eur. J.* **2016**, *22*, 32.
- [4] B. Pivovar, N. Rustagi, S. Satyapal, *Electrochem. Soc. Interface* **2018**, *27*, 47.
- [5] C. J. Quarton, O. Tlili, L. Welder, C. Mansilla, H. Blanco, H. Heinrichs, J. Leaver, N. J. Samsatli, P. Lucchese, M. Robinius, S. Samsatli, *Sustainable Energy Fuels* **2020**, *4*, 80.
- [6] E. Vartiainen, C. Breyer, D. Moser, E. Román Medina, C. Busto, G. Masson, E. Bosch, A. Jäger-Waldau, *Sol. RRL* **2021**, *6*, 2100487.
- [7] J. Schneidewind, *Adv. Energy Mater.* **2022**, *12*, 2200342.
- [8] IEA (2021), *Global Hydrogen Review*, OECD Publishing, Paris **2021**, <https://doi.org/10.1787/39351842-en>.
- [9] A. C. Nielander, M. R. Shaner, K. M. Papadantonakis, S. A. Francis, N. S. Lewis, *Energy Environ. Sci.* **2015**, *8*, 16.
- [10] T. J. Jacobsson, V. Fjällström, M. Edoff, T. Edvinsson, *Energy Environ. Sci.* **2014**, *7*, 2056.
- [11] B. Moss, O. Babacan, A. Kafzas, A. Hankin, *Adv. Energy Mater.* **2021**, *11*, 2003286.
- [12] H. Nishiyama, T. Yamada, M. Nakabayashi, Y. Maehara, M. Yamaguchi, Y. Kuromiya, Y. Nagatsuma, H. Tokudome, S. Akiyama, T. Watanabe, R. Narushima, S. Okunaka, N. Shibata, T. Takata, T. Hisatomi, K. Domen, *Nature* **2021**, *598*, 304.
- [13] K. R. Tolod, S. Hernández, N. Russo, *Catalysts* **2017**, *7*, 13.
- [14] S. Temburne, F. Nandjou, S. Haussener, *Nat. Energy* **2019**, *4*, 399.
- [15] J. H. Kim, D. Hansora, P. Sharma, J.-W. Jang, J. S. Lee, *Chem. Soc. Rev.* **2019**, *48*, 1908.
- [16] S. Ardo, D. Fernandez Rivas, M. A. Modestino, V. Schulze Greiving, F. F. Abdi, E. Alarcon Llado, V. Artero, K. Ayers, C. Battaglia, J.-P. Becker, D. Bederak, A. Berger, F. Buda, E. Chinello, B. Dam, V. Di Palma, T. Edvinsson, K. Fujii, H. Gardeniers, H. Geerlings, S. M. Hashemi, S. Haussener, F. Houle, J. Huskens, B. D. James, K. Konrad, A. Kudo, P. P. Kunturu, D. Lohse, B. Mei, E. L. Miller, G. F. Moore, J. Muller, K. L. Orchard, T. E. Rosser, F. H. Saadi,

- J.-W. Schüttauf, B. Seger, S. W. Sheehan, W. A. Smith, J. Spurgeon, M. H. Tang, R. van de Krol, P. C. K. Vesborg, P. Westerik, *Energy Environ. Sci.* **2018**, *11*, 2768.
- [17] I. Holmes-Gentle, S. Tembhurne, C. Suter, S. Haussener, *Int. J. Hydrogen Energy* **2021**, *46*, 10666.
- [18] A. Fallisch, L. Schellhase, J. Fresko, M. Zedda, J. Ohlmann, M. Steiner, A. Bösch, L. Zielke, S. Thiele, F. Dimroth, T. Smolinka, *Int. J. Hydrogen Energy* **2017**, *42*, 26804.
- [19] İ. B. Pehlivan, J. Oscarsson, Z. Qiu, L. Stolt, M. Edoff, T. Edvinsson, *iScience* **2021**, *24*, 101910.
- [20] M. Lee, B. Turan, J. Becker, K. Welter, B. Klingebiel, E. Neumann, Y. J. Sohn, T. Merdzhanova, T. Kirchartz, F. Finger, U. Rau, S. Haas, *Adv. Sustainable Syst.* **2020**, *4*, 2000070.
- [21] E. Kemppainen, S. Aschbrenner, F. Bao, A. Luxa, C. Schary, R. Bors, S. Janke, I. Dorbandt, B. Stannowski, R. Schlatmann, S. Calnan, *Sustainable Energy Fuels* **2020**, *4*, 4831.
- [22] S. Calnan, R. Bagacki, F. Bao, I. Dorbandt, E. Kemppainen, C. Schary, R. Schlatmann, M. Leonardi, S. A. Lombardo, R. G. Milazzo, S. M. S. Privitera, F. Bizzarri, C. Conelli, D. Consoli, C. Gerardi, P. Zani, M. Carmo, S. Haas, M. Lee, M. Mueller, W. Zwaygardt, J. Oscarsson, L. Stolt, M. Edoff, T. Edvinsson, I. B. Pehlivan, *Sol. RRL* **2022**, *6*, 2100479.
- [23] M. Gül, E. Akyüz, *Energies* **2020**, *13*, 2997.
- [24] S. Senthilraja, R. Gangadevi, H. Köten, R. Marimuthu, *Heliyon* **2020**, *6*, e05271.
- [25] F. Bao, E. Kemppainen, I. Dorbandt, R. Bors, F. Xi, R. Schlatmann, R. Krol, S. Calnan, *ChemElectroChem* **2021**, *8*, 195.
- [26] A. Thommes, W. Stark, W. Bacher, Die Galvanische Abscheidung von Eisen-Nickel In LIGA-Mikrostrukturen, PhD thesis, Karlsruher Institut für Technologie (KIT, Karlsruhe Institute of Technology), Karlsruhe, Germany **1995**, <https://doi.org/10.5445/IR/17795>.
- [27] I. Y. Ahmet, Y. Ma, J.-W. Jang, T. Henschel, B. Stannowski, T. Lopes, A. Vilanova, A. Mendes, F. F. Abdi, R. van de Krol, *Sustain. Energy Fuels* **2019**, *3*, 2366.
- [28] F. Bao, *NiMo and NiFeOx Electrocatalysts for Water Splitting*, PhD thesis, Technische Universität Berlin, Berlin, Germany **2021**, <https://doi.org/10.14279/depositononce-12200>.
- [29] A. Hankin, F. E. Bedoya-Lora, C. K. Ong, J. C. Alexander, F. Petter, G. H. Kelsall, *Energy Environ. Sci.* **2017**, *10*, 346.
- [30] F. Bao, E. Kemppainen, I. Dorbandt, F. Xi, R. Bors, N. Maticic, R. Wenisch, R. Bagacki, C. Schary, U. Michalczyk, P. Bogdanoff, I. Lauerermann, R. van de Krol, R. Schlatmann, S. Calnan, *ACS Catal.* **2021**, *11*, 10537.
- [31] G. Bender, M. Carmo, T. Smolinka, A. Gago, N. Danilovic, M. Mueller, F. Ganci, A. Fallisch, P. Lettenmeier, K. A. Friedrich, K. Ayers, B. Pivovar, J. Mergel, D. Stolten, *Int. J. Hydrogen Energy* **2019**, *44*, 9174.
- [32] T. Malkov, A. Pielnga, G. Tsotridis, G. De Marco, *EU Harmonised Polarisation Curve Test Method For Low-Temperature Water Electrolysis*, European Commission, Joint Research Centre **2018**, <https://doi.org/10.2760/179509>.
- [33] D. Le Bideau, P. Mandin, M. Benbouzid, M. Kim, M. Sellier, *Int. J. Hydrogen Energy* **2019**, *44*, 4553.
- [34] Instruction Manual: Mass Flow/Pressure meters and controllers for gases and liquids, https://www.bronkhorst.com/getmedia/4f45d04f-4704-424f-8172-0bfb95d93d6a/917001manual_mass_flow_pressure_meters_controllers.pdf (accessed: November 2019).
- [35] *CRC Handbook of Chemistry and Physics*, 95th ed. (Ed: W. M. Haynes), CRC Press, Boca Raton, Florida, USA **2014**, <https://doi.org/10.1201/b17118>.
- [36] R. Usamentiaga, P. Venegas, J. Guerediaga, L. Vega, J. Molleda, F. G. Bulnes, *Sensors* **2014**, *14*, 12305.
- [37] J. W. Haverkort, H. Rajaei, *J. Power Sources Adv.* **2020**, *6*, 100034.
- [38] M. Müller, W. Zwaygardt, *PECSYS Project Deliverable Report - D7.6: Final Report About System Performance Including Report About MS5* **2021**, <https://cordis.europa.eu/project/id/735218/results>.
- [39] S. Tembhurne, S. Haussener, *Sustainable Energy Fuels* **2019**, *3*, 1297.